

Comparing Hyper-optimized Machine Learning Models for Predicting Efficiency Degradation in Organic Solar Cells

David Valiente^{a,b,*}, Fernando Rodríguez-Mas^b, Juan V. Alegre-Requena^c,
David Dalmau^c, Juan C. Ferrer^a

^a*University Institute for Engineering Research, Miguel Hernandez University, Avenida de la Universidad, s/n, Elche, 03202, Spain*

^b*Communications Engineering Department, Miguel Hernandez University, Avenida de la Universidad, s/n, Elche, 03202, Spain*

^c*Institute of Chemical Synthesis and Homogeneous Catalysis (ISQCH), CSIC, University of Zaragoza, Pedro Cerbuna 12, Zaragoza, 50009, Spain*

Abstract

This work presents a set of optimal machine learning (ML) models to represent the temporal degradation suffered by the power conversion efficiency (PCE) of polymeric organic solar cells (OSCs) with a multilayer structure ITO/PEDOT:PSS/P3HT:PCBM/Al. To that aim, we generated a database with 996 entries, which includes up to 7 variables regarding both the manufacturing process and environmental conditions for more than 180 days. Then, we relied on a software framework that brings together a conglomeration of automated ML protocols that execute sequentially against our database by simply command-line interface. This easily permits hyper-optimizing and randomizing seeds of the ML models through exhaustive benchmarking so that optimal models are obtained. The accuracy achieved reaches values of the coefficient determination (R^2) widely exceeding 0.90, whereas the root mean squared error (RMSE), sum of squared error (SSE), and mean absolute error (MAE) $\leq 1\%$ of the target value, the PCE. Additionally, we contribute with validated models able to screen the behavior of OSCs never seen in the database. In that case, $R^2 \sim 0.96-0.97$ and $RMSE \sim 1\%$, thus confirming the reliability of the proposal to predict. For comparative purposes, classical Bayesian regression fitting based on non-linear mean squares (LMS) are also presented, which only perform sufficiently for univariate cases of single OSCs. Hence they fail to outperform the breadth of the capabilities shown by the ML models. Finally, thanks to the standardized results offered by the ML framework, we study the dependencies between the variables of the dataset and their implications for the optimal performance and stability of the OSCs. Reproducibility is ensured by a standardized report altogether with the dataset, which are publicly available at Github¹.

Keywords: Organic solar cell, Degradation, P3HT:PCBM, PEDOT:PSS,

*Corresponding author

Email addresses: dvaliente@umh.es (David Valiente), fernando.rodriguez@umh.es (Fernando Rodríguez-Mas), jvalegre@unizar.es (Juan V. Alegre-Requena), ddalmau@unizar.es (David Dalmau), jc.ferrer@umh.es (Juan C. Ferrer)

¹<https://github.com/davidumh11>

1. Introduction

Nowadays electricity consumption has evolved exponentially over the last three decades, increasing from a total estimate of 15107.8 TWh to 28661 TWh between 2000 and 2022, respectively [1]. One of the immediate consequences has been reflected in the price of this energy. Simultaneously, in the technological realm, there has been a notable shift in electricity generation towards renewable sources. Particularly, the maturity of conventional photovoltaic (PV) cells and the emergence of new organic and hybrid materials have made possible to get significant improvements in PV generation and its power conversion efficiency (PCE) [2]. However, despite the fact that the global consumption of PV energy increases from 1.08 TWh to 1310.02 TWh between 2000 and 2022 [1], its generation still falls short of meeting current demand. Hence, there are many challenges and open lines for improving the generation and efficiency of PV cells.

In this context, organic solar cells (OSCs) have emerged as a promising alternative to silicon-based solar cells since, amongst other benefits, their production involves low-temperature manufacturing methods [3], reducing their carbon footprint. Their appeal also lies in the ease of processing, low cost, flexibility, and lightweight [4]. Moreover, the evolution of their PCEs has been much superior to classical technologies and it has been on par with other considered emerging technologies, presenting efficiencies that exceed values of 20% [5]. However, the commercialization of OSCs still faces various challenges, including stability and efficiency. Nevertheless, certain cost studies [6, 7] indicate that once these obstacles are overcome, OSCs can be manufactured at a cost lower than 1 dollar per peak Watt [8]. This fact suggests that the optimization of the manufacturing procedure of these organic devices would certainly lead to reinforce their benefits, but also, and most importantly, their sustainability and stability to operate long-term feasibly. All in all, the potential capabilities of artificial intelligence (AI) protocols, through particular machine learning (ML)-based models, envisages great achievements in this sense.

The integration of ML before transferring to industrial implementation it is being extensively tested these days. For instance, within the field of cheminformatics, it is of paramount importance in the design of new materials. Numerous studies have demonstrated the potential of deep learning algorithms to analyze complex chemical data, thereby accelerating the process of discovering, for example, drugs, as well as identifying promising compounds with improved properties [9]. Some of the early studies [10, 11] laid the foundations for the application of ML models in predicting molecular properties, highlighting their great strengths. More recently, the deployment of AI techniques with high-performance prediction methods has enabled the emergence of software platforms capable of examining extensive chemical databases to identify potential materials with significant properties [12, 13]. A relevant database, which moved forward from general chemical structures to the inclusion of PV features was the

project presented in [14]. This work allowed to obtain custom predictive models that characterize the electrical behavior of PV devices in terms of parameters such as voltage, current, conversion efficiency, short-circuit current, open-circuit voltage, etc. [15, 16, 17, 18]. Thus there is an endless list of mathematical models mostly supported by ML and deep learning-based engines that combine different techniques, such as regression and statistical inference [19, 15, 20, 21, 22] to optimize different target features of optoelectronic devices [23, 24, 25]. Similarly, the growth of proposals with eco-design characteristics and AI support for the production of sustainable and durable energy generating materials is positively evolving [26, 27, 28]. More specifically, some studies have trusted on ML for predicting optimal installation of energy harvesting systems [29, 30, 31] and consequently on predicting energy generation [32, 33, 30]. Similarly, fault detection of these systems were also anticipated thanks to automated models [34, 35]. Others delved into the manufacturing variables of their specific structures [36, 37, 38, 39]. In the same way, there is incipient research on the analysis of stability and durability of these devices [40, 41, 42, 43].

In sight of all these developments, this work explores different ML models to encode the PCE performance of polymeric OSCs based on multilayer ITO/PEDOT:PSS/P3HT:PCBM/Al. This permits producing models that reliably learn from the PCE evolution over time. Furthermore, several dependencies on the variables involved in the manufacturing [44], but also on the environmental conditions [45, 46, 47], are also learnt by these models. To that aim, we have used an hyper-optimizer software, ROBERT [48], that permits benchmarking with multiple ML models and so that to produce extensive and standardized results, which are generated with optimal methods. Our dataset consists of PCE measurements of 45 OSC devices with variability in up to 7 variables, acquired for more than 180 days. This means a database with 996 entries. The accuracy metrics demonstrate the validity of these models to learn and represent the temporal behavior of our OSCs, with determination coefficient up to $R^2=0.96$, and root mean squared error (RMSE), sum of squared error (SSE) and mean absolute error (MAE) bounded around 1% of the target value, that is, the PCE. Additionally, traditional Bayesian regression models sustained by LMS have been introduced in order to confirm the advantages of the ML-automated protocols against these classical approaches. While these conventional methodologies such as [49, 50, 51] may yield satisfactory results in this domain, our approach demonstrates that the potential of computational learning modeling offers a much broader and comprehensive solution compared to those based on classical statistical models, showcasing, among other benefits, increased robustness and reliability for:

- Capturing multivariate relationships between variables, encompassing both linear and non-linear relationships.
- Learning from an entire dataset, not solely from a specific OSC device as in classical regression.
- Screening new OSC devices not used during the learning phase, thereby

predicting its behavior, as an unknown device.

- Predicting optimal variables to fabricate the OSC that maximizes the PCE and/or its stability over time.

In contrast ML models, typical statistical algorithms are unable to predict; instead, they utilize estimations to extrapolate target values to immediately subsequent time instances, which must also be exclusive to a particular OSC rather than to an entire database with variability across different variables.

In summary, the key contributions of this research are as follows:

1. Assessment of optimal ML models that learn the PCE behavior over time for polymer-based OSC devices with ITO/PEDOT:PSS/P3HT:PCBM/Al structure, considering various fabrication variables and environmental measurement conditions.
2. Comparative benchmarking among different ML models and classical statistical regression approaches.
3. Identification of an optimal ML model capable of accurately predicting the PCE behavior of unseen OSC devices, unknown during the training and validation phases.
4. Analysis of dependencies among the dataset variables to establish influence on the performance of the OSCs devices and their fabrication.
5. Reproducibility and transparency of the obtained ML models using a standardized framework for command line replication.

The rest of the paper is organized as follows: Section 2 describes the specific OSCs manufactured in our laboratory, their electrical parameters, and the periodic measurements that comprise the database used by the ML methods. Subsequently, these methods are defined, starting from a preliminary scope of regression problems, along with the software framework that enables their benchmarking and, consequently, the extraction of models with optimal hyperparameters. Then, Section 3 outlines the experiments and results. Finally, Section 4 draws conclusions from this work.

2. Materials and Methods

2.1. Organic Solar Cells

The OSCs characterized in this work are manufactured through the spin-coating technique, which involves the deposition of overlapped polymeric thin films. Polymers are deposited in solution, then a process of rotation followed by heating aids in removing the solvent, hence forming the layer. The structure of the devices was as follows: ITO/PEDOT:PSS/P3HT:PCBM/Al, where each layer refers to:

- ITO: Indium tin oxide.

- PEDOT:PSS: poly(3,4-ethylenedioxythiophene) polystyrene sulfonate.
- P3HT:PCBM: (poli(3-hexiltiofeno-2,5-diil):[6,6]-phenyl-C61-butyric acid methyl ester.
- Al: Aluminium.

As a substrate, a glass with a 60 nm thick semi-transparent ITO layer was used. The substrates are placed in the spinner with the ITO layer facing upwards so that the thin layers can be deposited on it. The first layer deposited was the PEDOT:PSS film. PEDOT:PSS was deposited at room temperature at a rotation speed of 6000 rpm for 60 seconds. The remaining solvent was removed by heating at 150°C for ten minutes. Once the first layer was deposited, the active layer composed by the P3HT:PCBM polymer blend was applied. This was done at 300 rpm for three minutes. It was then dried at 80°C for one hour.

The final layer deposited on the devices is the aluminium film. Aluminium is not deposited using the spin-coating technique but rather by metal evaporation in a vacuum chamber. The equipment consists of a high vacuum chamber, two vacuum pumps, one of which is a high vacuum pump, and a power supply to provide the necessary current to evaporate the aluminium. Once the samples are placed inside the chamber, vacuum is achieved, reaching pressures of 10^{-6} mbar. Once this pressure is reached, aluminium is evaporated by Joule effect.

2.2. OSC database

As initially mentioned in Section 1, our dataset consists of PCE measurements of 45 OSC devices where up to 7 variables are registered for more than 180 days. Electrical parameters (J-V curves) of these OSCs are acquired along with climate conditions. The acquisition process comprises a Keithley-2400 equipment that acts as source generator for the voltage sweep as well as recorder of the generated PV current. The J-V curves have to be measured under light conditions (100 mW/cm², AM 1.5G, and 25°C) generated by a solar simulator Newport xenon arc lamp and an AM 1.5G filter. The electrical characterization is completed by determining the characteristic electrical parameters, including the short-circuit current density (J_{sc}), the open-circuit voltage (V_{oc}), the maximum power point (P_{mpp}), the fill factor (FF), and the PCE. Obtaining these parameters allows to extract the PCE value as follows:

$$PCE = \frac{P_{mpp}}{P_{inc}} = \frac{J_{sc}V_{oc}FF}{G} \quad (1)$$

being P_{inc} the incident solar power on the OSCs, which derives from the incident irradiance of the solar simulator, G .

The block diagram of the equipment for the acquisition system is presented by Figure 1. This permitted obtaining a database with 996 entries. The variables and their units are presented by Table 1.

As an example, Figure 2 presents an OSC contained in the database, for which its current density (J) data have been periodically acquired against voltage (V) over 78 days. Specifically, Figure 2(a) displays the voltage range on the

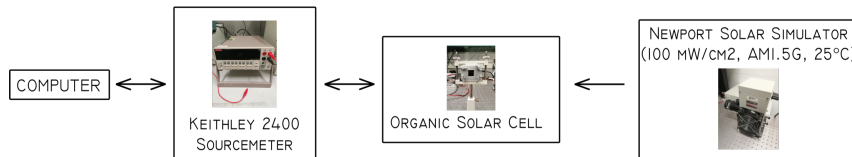


Figure 1: Block diagram of the acquisition system used to generate the OSC database.

Table 1: Variable details of the dataset.

Variables	Values
Cell name	[1-5]
solvent quantity HTL (PEDOT:PSS) [μ l]	[250-1000]
P3HT [mg]	[1-1.2]
PCBM [mg]	[0.8-1]
Volume ratio P3HT:PCBM	[1-1.25]
Temperature [$^{\circ}$ C]	[12-23]
Hummidity [%]	[33-88]
Dew point [$^{\circ}$ C]	[3-19]
Pressure [hPa]	[997-1022]
Time [days]	[0-181]

X-axis from 0 to 0.5 V, while Figure 2(b) adjusts the scale to show the range from 0 to 0.25 V, allowing for a clearer observation of the evolution of the J-V curve as the days pass by. The degradation principles of these organic devices suggest that over time, these curves, from which maximum power and energy conversion efficiency are obtained, should consistently decline. However, it can be observed in Figure 2(b) that there are certain temporal points between days 20, 26, 47 and 69, where the current density associated with specific voltages remains close to, or even exceeds, the current density associated with those same voltages but at earlier temporal points. This outline confirms that rather than time, there are other variables influencing the degradation of these devices, which implies that a specific OSC could exhibit slightly better performance in the future under certain conditions.

In the same manner, Figure 3 compares the temporal evolution of three different OSCs in terms of their normalized PCE values, ranging from 0 to 1, for more than 180 days. Once again, it is confirmed that time leads to the degradation of the device’s conversion efficiency. However, it also emerges that differences in the fabrication of the various OSCs, as well as the environmental conditions during their measuring, may influence the trend followed by the PCE over time.

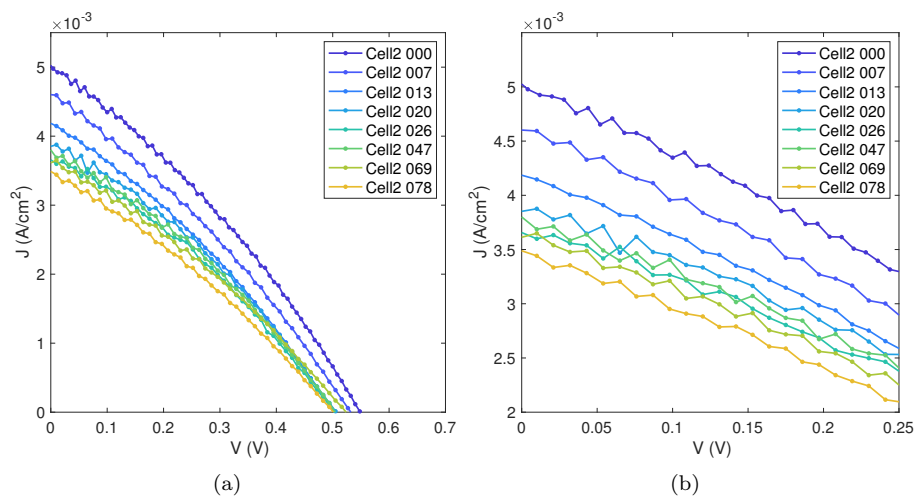


Figure 2: Evolution of current density (J) vs. voltage (V) over time (days) for the OSC *Cell2*. (a) Curve J - V with $V \in [0-0.7]$ V. (b) Same curve J - V with $V \in [0-0.25]$ V.

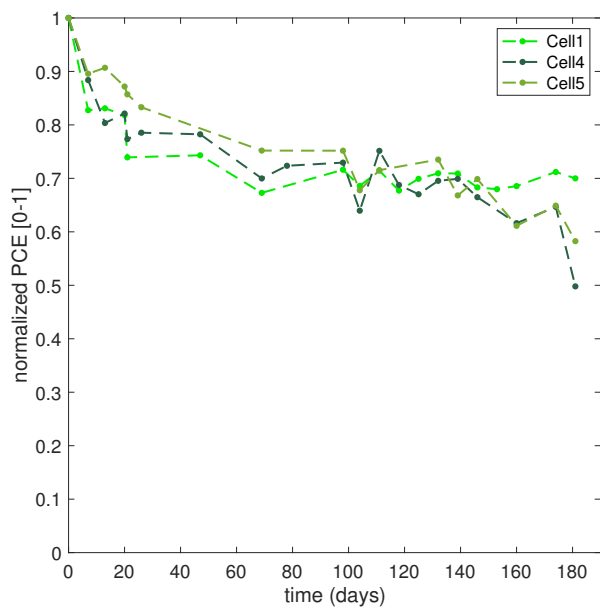


Figure 3: Evolution of the normalized PCE over time for three different OSCs.

2.3. Regression Problem

As already stated, this study aims to automatically model the degradative behavior exhibited by manufactured OSCs using ML approaches. It is clear that we deal with a regression problem, for which recent literature has demonstrated that is reliably and efficiently solved by computational learning. However, in order to establish further comparisons that highlight and reinforce the abilities of AI-based protocols, a preliminary step is carried out to present regression fitting using traditional LMS-supported Bayesian methods.

Regression is a method for estimating the relationship between a response or output variable and one or more predictor or input variables. Linear and non-linear regression serve as estimators of values between observed data points. From that starting point, a regression model relates response data to predictor data through one or more coefficients. Then a fitting algorithm is needed to calculate some model coefficients from a set of input data. In this sense, parametric fitting involves finding those coefficients, assuming that the data are statistical composed by deterministic and random components. Therefore, the parametric model estimates the deterministic component, whereas the random component is typically described as the error. Considering the model as a coefficient function of the independent variable, the error encodes random fluctuations around a Gaussian probability distribution. In many scopes, the goal is to minimize that error, classically addressed by means of LMS fitting approaches, such as: linear least squares, weighted least squares, robust least squares, non-linear least squares, etc.

$$y = f(X, \beta) + \varepsilon \quad (2)$$

where y is the output vector data of $n \times 1$, corresponding to the input data in X of $n \times m$, after being applied f as a non-linear function of the coefficient vector β ($m \times 1$), being ε the vector of unknown errors of $n \times 1$. Afterwards, the SSE is minimized, understood as the residual sum of squares, given a set of n data values, the residual value of the i -th value r_i is calculated as:

$$r_i = y_i - \hat{y}_i \quad (3)$$

where y_i represents the i -th observed value and \hat{y}_i represents the i -th estimated value, and accordingly:

$$SSE = \sum_{i=1}^n r_i^2 = \sum_{i=1}^n (y_i - \hat{y}_i)^2 \quad (4)$$

Subsequently, the algorithm proceeds iteratively calculating the coefficients from an initial seed. Sometimes non-linear models trust on heuristic schemes to calculate initial values. For others models, coefficients randomly initialized in ranges from [0-1]. Then the response value is given as $\hat{y} = f(X, \beta)$, computed using the jacobian matrix of $f(X, \beta)$, as the matrix that contains the partial derivatives with respect to the coefficients of β . Finally, the adjustment of the coefficients for the next iteration lies on some non-linear least squares algorithms, such as Levenberg-Marquardt, Gradient descent or Gauss-Newton [52]. Whenever the

fitting meets the specified convergence criteria, the final solution is assumed as valid.

After observing in Section 2.2 the behavior of PCE over time for the various OSCs contained in our database, it was validated that the LMS regression fitting models yielding the best results were those with non-linear characterization. Table 2 displays the selected models along with their expressions as a function of time, dependent on the adjustment coefficients. It should be noted that the capability of these classical models lies solely in modeling the univariate behavior of the time effect on the PCE values. While it is possible to explore other LMS regression fitting in the multivariate domain, they only allow for establishing linear relationships, which do not adequately capture the behavior of our devices.

Table 2: LMS Bayesian regression fitting models to estimate PCE, denoted as $f(x)$, where x represents time by means of parametric models.

Parametric model	Coefficient expression of $f(x)$
<i>exp1</i>	ae^{bx}
<i>exp2</i>	$a\epsilon^{bx} + ce^{dx}$
<i>gauss1</i>	$a_1e^{-[(x-b_1)/c_1]^2}$
<i>gauss2</i>	$a_1e^{-[(x-b_1)/c_1]^2} + a_2e^{-[(x-b_2)/c_2]^2}$
<i>poly3</i>	$p_1x^3 + p_2x^2 + p_3x + p_4$

2.4. Machine Learning framework

In contrast to the previous classical approaches, ML moves forward to produce non-parametric regression models that adjust more complex behaviors without specifying the relationship between the output and input data by certain predetermined regression function. They may simply predict responses with new test data using a trained model. In this work, we exploit the advantages of a software framework, ROBERT [48], developed under Python that facilitates hyper-optimization and benchmarking over well-recognized ML regression models by single command line instruction. This framework consists of the following modules:

- Data curation: It processes the target dataset in order to filter correlated descriptors, noise, duplicates, as well as to identify and to convert categorical variables into one-hot descriptors.
- Model selection: It iterates through multiple hyper-optimized models from scikit-learn [53]. It includes training size analysis by varying data partitions percentages (training-validation) and it also examines different data splitting options like k-neighbors clustering-based (KN) and random (RND). Permutation feature importance (PFI) detection is also performed. In consequence, models are computed with PFI-filtered descriptors and without them. As a default setting, this threshold eliminates features whose contribution to the model’s R^2 is less than 4%. Moreover,

it provides with insights on the dependencies of the input variables, thanks to SHapley Additive exPlanations (SHAP) analysis. Besides this, heatmap graphics are presented in order to compare models in terms of RMSE error. Amongst the generated models, it assesses the performance of Random Forests (RF), Multivariate Linear Models (MVL), Gradient Boosting (GB), Gaussian Process (GP), AdaBoost Regressor (AdaB), MLP Regressor Neural Network (NN), and Voting Regressor (VR) [53].

- Prediction: Once the models are trained and validated, the framework permits external test sets to predict target values with the best models.
- Verify module: It assesses the predictive ability of the models, considering tests such as y-shuffle, y-mean, k-fold cross-validation, and one-hot features prediction.
- Report module: With the aim of providing reproducibility and transparency, this module offers a detailed report containing comprehensive information about the ML models utilized and replication instructions through command line executions.

As an example of performance, Figure 4 illustrates the result obtained by ROBERT with our dataset as input data. Specifically, Figure 4(a) and Figure 4(b) compare the evolution exhibited by the ML models over time. The first figure depicts the result of a single model for training data up to 30 days, while the second figure does the same for training data up to 180 days. Their validity can be checked by inspecting the predicted outcome against the target values used as training (blue) and validation (yellow) data.

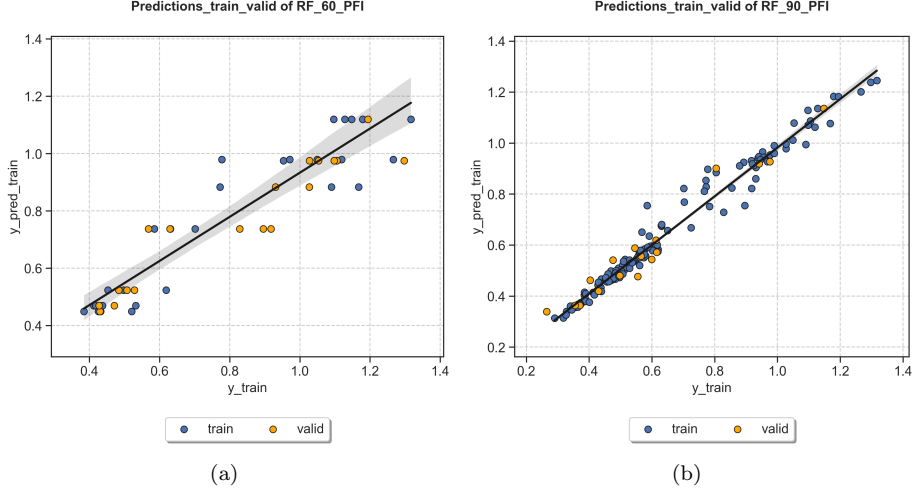


Figure 4: Results of the best ML models, tested with training (blue) and validation (yellow) target data up to: (a) 30 days and (b) 180 days.

3. Results

This section introduces the results obtained using both classical LMS regression fitting models and the optimal ML models as generated by the framework used in this work, to estimate the temporal behavior of our OSCs. The selected error metrics for analysis are briefly presented below:

- Coefficient of determination R^2 : It quantifies how well the independent variables explain the variability of the dependent variable. Higher values indicate that the model fits the data well and captures larger proportion of the variability in the dependent variable.

$$R^2 = 1 - \frac{SSE}{SS_{tot}} \quad (5)$$

- RMSE: It provides a measure of the average magnitude of the errors made by the model in its predictions. Minimizing this error is often a goal when training regression models in ML.

$$RMSE = \sqrt{\frac{1}{n} \sum_{i=1}^n (y_i - \hat{y}_i)^2} \quad (6)$$

- MAE: Another common objective error that measures the average magnitude of the errors between the predicted values and the actual values of

the target variable. Unlike RMSE, which penalizes large errors more heavily, MAE treats all errors equally by taking the average of their absolute values. This makes MAE more robust to outliers in the data compared to RMSE.

$$MAE = \frac{1}{n} \sum_{i=1}^n |y_i - \hat{y}_i| \quad (7)$$

Meanwhile, SSE was defined in (4) and SS_{tot} is the total sum of squares, whereas n is the number of samples, y_i is the real observed value and \hat{y}_i is the predicted value.

3.1. Classical LMS regression fitting results

Hence, Figure 5 presents the accuracy metrics of the five Bayesian regression models introduced in Table 2 to estimate the performance of PCE over 180 days, for each of the OSCs available in the database (Table 1). It is worth noting that these results correspond to the mean values, along with the standard deviation for each OSC. Specifically, the values of R^2 are shown in Figure 5(a), RMSE in Figure 5(b), SSE in Figure 5(c), and MAE in Figure 5(d). It can be observed that these models perform effectively when the temporal range of the fitting data is limited: as long as the time goes by, all models experience an increase in error, while R^2 decreases. According to the results of Figure 5, it is observed that on average, the *gauss2* model, consisting of two Gaussian terms, is the one that best estimates the performance of the OSCs in terms of PCE over time. However, it should be noted that for a 30 day fit, this model requires more points to achieve a valid R^2 . On the other hand, it should be pointed out that the maximum errors for all temporal fittings are bounded to values ~ 0.06 , fact that represents an error $>1\%$ of the the target value, the PCE. Notwithstanding that, it must be reiterated the limitation of these methods to characterize the behavior of all devices contained in our database in a global manner. These results reflect solely the mean performance of fitting for single OSCs, in turn.

3.1.1. PCE fitting estimation

Once preliminary fitting have been made with traditional LMS regression methods, it has been found that the best fitting corresponds to a double-term Gaussian function. Now we analyze the robustness of this method to estimate the behavior of PCE against the temporal variable. For this purpose, different estimations have been obtained, as shown in Figure 6. This figure presents estimated PCE data from a specific OSC device, namely *Cell4* in our databased, which has been used so far in the all the previous examples throughout this work. Here, the parametric model is obtained with fitting data at: 30, 60, 90, and 120 days, respectively. Then the behavior of PCE at 180 days has been estimated, in order to be tested against the real data of the database. It can be observed that the estimated trend for fitting models with 30, 60, and 90 days deviate considerably from the real behavior (represented by the black line). It can be concluded that fitting data up to at least 120 days are required to make

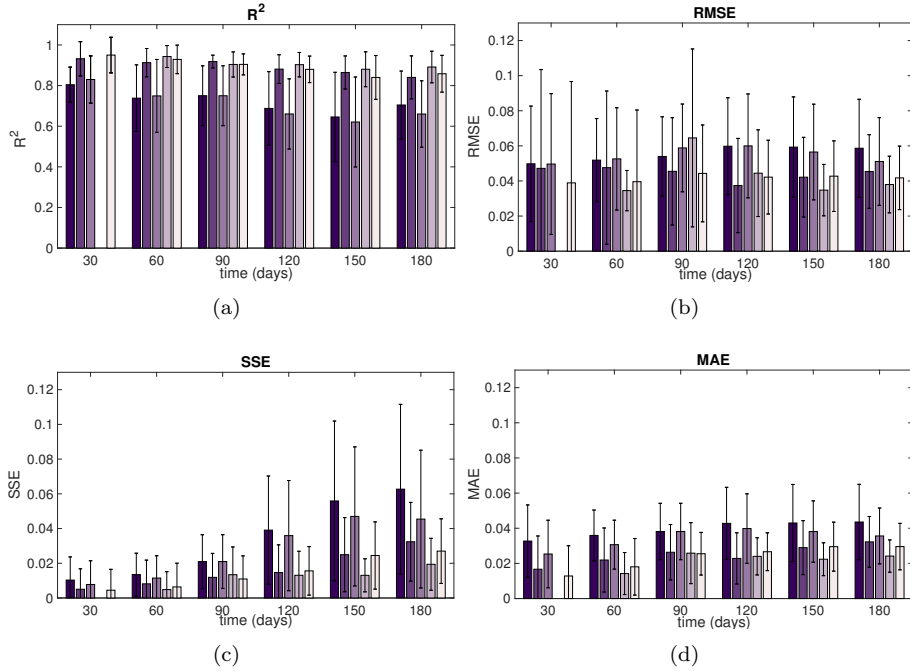


Figure 5: Accuracy metrics of the LMS-supported Bayesian regression fitting over time. Five different models are evaluated: *exp1* (dark blue), *exp2* (medium blue), *gauss1* (purple), *gauss2* (light purple), *poly3* (pink). (a) Coefficient of determination, R^2 . (b) Root mean squared error, RMSE. (c) Sum of squared errors, SSE. (d) Mean absolute error, MAE.

a robust fitting that achieves sufficient confidence in estimating future data at 180 days. This fact demonstrates that even the best parametric LMS fitting regression model requires more than half of the temporal data to reliably model the PCE evolution at future time values. In order to get further insights on the estimations plotted in Figure 6 more easily, Table 3 presents the specific details of these estimations according to the error metrics RMSE, SSE, and MAE. Upon inspection, the perception extracted from the previous figure is validated: the errors are unacceptable for any metric unless the fit is made with more than half of the data (90 days), and only if the subsequent PCE estimation is tested over time values immediately posterior to the temporal limit of the fitting.

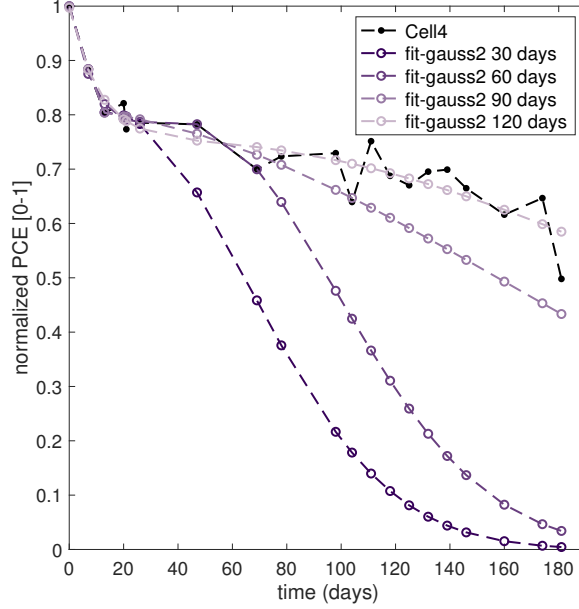


Figure 6: PCE estimation over time with the best LMS-supported Bayesian regression fitting model (*gauss2*). Four temporal datasets are used to compute the fittings: 30 days $- \circ -$; 60 days $- \circ -$; 90 days $- \circ -$ and 120 days $- \circ -$.

Table 3: Accuracy metrics of the best LMS-supported Bayesian regression fitting model (*gauss2*) to estimate PCE over time, presented in Fig 6.

Fitting data	Estimation	RMSE	SSE	MAE
30 days	60 days	0.0516	0.0213	0.0277
	90 days	0.1141	0.1302	0.0680
	120 days	0.1872	0.4905	0.1339
	150 days	0.2224	0.8405	0.1705
	180 days	0.2442	1.3117	0.1979
60 days	90 days	0.0454	0.0206	0.0220
	120 days	0.1083	0.1641	0.0685
	150 days	0.1511	0.3879	0.1046
90 days	120 days	0.0150	0.0032	0.0103
	150 days	0.0160	0.0043	0.0119
	180 days	0.0190	0.0079	0.0118
120 days	150 days	0.0158	0.0042	0.0127
	180 days	0.0138	0.0038	0.0105

3.2. Machine Learning regression results

In this section, we conduct the generation of ML models to learn from the temporal behavior of PCE versus time. It is noteworthy that, unlike the previous

LMS-based regression fittings presented in Section 3.1, these ML models allow us to characterize the performance of our devices in a multivariate manner, thereby encoding the variability presented in their manufacturing, as well as in the particular environmental conditions at each temporal measurement, as indicated in Table 2.

Thanks to the use of the tool ROBERT [48], we achieve an exploration of various combinations of ML algorithms and partition sizes. In order to maintain the same accuracy estimation policy used in Section 3.1, Figure 7 presents the same metrics as Figure 5. In this case, for each temporal training dataset (X-axis), the coefficient R^2 is presented in Figure 7(a), RMSE in Figure 7(b), SSE in Figure 7(c), and MAE in Figure 7(d), for the best ML model in each case. It can be observed that, in general, all errors are bounded approximately within ranges $\sim[0.02-0.03]$, for training data of 120 days onwards. This implies an error percentage lower than 1%, with respect to the mean value of PCE for these OSCs, which is highly satisfactory for modeling. It is also worth noting the good performance of the RF model, with training-validation partitions of 90-10%.

So as to comparatively assess the remaining ML models, Tables 4, 5, 6, 7, 8, and 9, respectively present detailed accuracy results for the other models (GB, NN, MVL, and RF). Results with different training-validation ratios are presented: from 90-10% to 60-40%; while training data range from 30 to 180 days. For each table, the robustest model is highlighted in bold, considering the overall performance across all presented metrics, with priority given to the R^2 value. It is worth mentioning that, even though they are not directly comparable models, it is confirmed that the errors of the ML methods are clearly bounded, while the LMS-based fitting regression errors grow with time. Furthermore, ML models have the ability to globally model a multivariate database, in contrast to univariate Bayesian fitting, which is independent for each device.

Table 4: Accuracy metrics of the Machine Learning regression models computed with training data up to 30 days.

Training data	ML model	R^2	RMSE	SSE	MAE
30 days	GB-80-20	0.86	0.140	0.0647	0.1200
	GB-70-30	0.73	0.140	0.0622	0.1200
	GB-60-40	0.84	0.160	0.1103	0.1500
	NN-80-20	0.76	0.180	0.1655	0.1800
	NN-70-30	0.51	0.170	0.0832	0.1600
	NN-60-40	0.62	0.170	0.0931	0.1400
	MVL-80-20	0.71	0.200	0.0984	0.1500
	MVL-70-30	0.62	0.220	0.1006	0.1400
	MVL-60-40	0.66	0.170	0.1067	0.1400
	RF-80-20	0.86	0.130	0.0573	0.1000
	RF-70-30	0.78	0.130	0.0558	0.1000
	RF-60-40	0.89	0.120	0.0725	0.0950

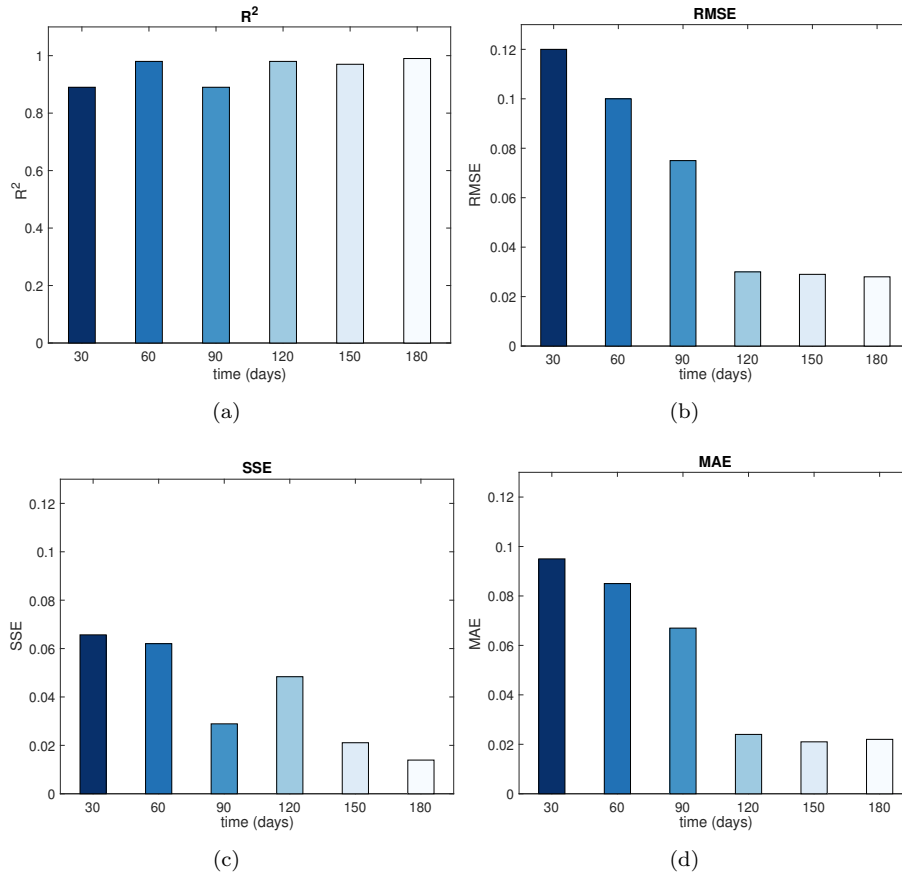


Figure 7: Accuracy of the best Machine Learning regression models over time: 30 days RF-60-10 ■; 60 days RF-90-10 ■; 90 days RF-90-10 ■; 120 days RF-90-10 ■; 150 days RF-90-10 ■ and 180 days RB-90-10 □. (a) Coefficient of determination, R^2 . (b) Root mean squared error, RMSE. (c) Sum of squared errors, SSE. (d) Mean absolute error, MAE.

Table 5: Accuracy metrics of the Machine Learning regression models computed with training data up to 60 days.

Training data	ML model	R ²	RMSE	SSE	MAE
60 days	GB-90-10	0.85	0.1000	0.0155	0.0800
	GB-80-20	0.76	0.1500	0.0433	0.1300
	GB-70-30	0.84	0.1500	0.0597	0.1300
	GB-60-40	0.78	0.1700	0.1275	0.1500
	NN-90-10	0.89	0.1300	0.1239	0.1000
	NN-80-20	0.86	0.1700	0.1677	0.1500
	NN-70-30	0.88	0.1500	0.0506	0.1300
	NN-60-40	0.79	0.1600	0.0677	0.1400
	MVL-90-10	0.71	0.1500	0.1059	0.1300
	MVL-80-20	0.80	0.1700	0.1120	0.1500
	MVL-70-30	0.63	0.1700	0.1117	0.1500
	MVL-60-40	0.61	0.1900	0.1290	0.1500
	RF-90-10	0.98	0.1000	0.0702	0.0850
	RF-80-20	0.92	0.1400	0.0832	0.1300
	RF-70-30	0.78	0.1600	0.0747	0.1400
	RF-60-40	0.81	0.1300	0.0578	0.1000

Table 6: Accuracy metrics of the Machine Learning regression models computed with training data up to 90 days.

Training data	ML model	R ²	RMSE	SSE	MAE
90 days	GB-90-10	0.87	0.0730	0.0255	0.0660
	GB-80-20	0.87	0.1100	0.0736	0.0860
	GB-70-30	0.88	0.0940	0.0775	0.0770
	GB-60-40	0.75	0.1400	0.0755	0.1100
	NN-90-10	0.86	0.0790	0.0332	0.0630
	NN-80-20	0.82	0.1300	0.1595	0.1200
	NN-70-30	0.46	0.1900	0.1071	0.1700
	NN-60-40	0.52	0.1900	0.1611	0.1500
	MVL-90-10	0.61	0.1100	0.3161	0.1000
	MVL-80-20	0.63	0.1700	0.1468	0.1400
	MVL-70-30	0.54	0.1700	0.1378	0.1400
	MVL-60-40	0.55	0.1800	0.1569	0.1500
	RF-90-10	0.89	0.0750	0.0300	0.0670
	RF-80-20	0.87	0.0940	0.0909	0.0700
	RF-70-30	0.80	0.1000	0.0613	0.0780
	RF-60-40	0.74	0.1400	0.0860	0.1100

Table 7: Accuracy metrics of the Machine Learning regression models computed with training data up to 120 days.

Training data	ML model	R ²	RMSE	SSE	MAE
120 days	GB-90-10	0.95	0.0670	0.0312	0.0540
	GB-80-20	0.88	0.0700	0.0324	0.0510
	GB-70-30	0.89	0.0810	0.0453	0.0620
	GB-60-40	0.81	0.1300	0.1447	0.1100
	NN-90-10	0.88	0.0600	0.2140	0.0450
	NN-80-20	0.83	0.0890	0.0576	0.0660
	NN-70-30	0.71	0.1300	0.0767	0.0960
	NN-60-40	0.59	0.1700	0.1743	0.1300
	MVL-90-10	0.70	0.0990	0.1729	0.0850
	MVL-80-20	0.65	0.1400	0.1820	0.1100
	MVL-70-30	0.60	0.1600	0.2311	0.1400
	MVL-60-40	0.51	0.1800	0.2370	0.1500
	RF-90-10	0.98	0.0300	0.0507	0.0240
	RF-80-20	0.88	0.0680	0.0651	0.0480
	RF-70-30	0.86	0.0920	0.0609	0.0690
	RF-60-40	0.84	0.1000	0.0574	0.0770

Table 8: Accuracy metrics of the Machine Learning regression models computed with training data up to 150 days.

Training data	ML model	R ²	RMSE	SSE	MAE
150 days	GB-90-10	0.98	0.0300	0.0510	0.0230
	GB-80-20	0.93	0.0660	0.0242	0.0420
	GB-70-30	0.94	0.0730	0.0351	0.0580
	GB-60-40	0.91	0.0820	0.0591	0.0640
	NN-90-10	0.90	0.0580	0.0760	0.0540
	NN-80-20	0.82	0.0110	0.1277	0.0630
	NN-70-30	0.88	0.0960	0.0871	0.0740
	NN-60-40	0.78	0.1200	0.1533	0.0910
	MVL-90-10	0.84	0.0920	0.2113	0.0800
	MVL-80-20	0.87	0.1100	0.2139	0.0840
	MVL-70-30	0.88	0.1200	0.2163	0.0900
	MVL-60-40	0.82	0.1100	0.2184	0.0910
	RF-90-10	0.97	0.0290	0.0219	0.0210
	RF-80-20	0.96	0.0510	0.0394	0.0324
	RF-70-30	0.94	0.0780	0.0417	0.0570
	RF-60-40	0.90	0.0930	0.1069	0.0943

Table 9: Accuracy metrics of the Machine Learning regression models computed with training data up to 180 days.

Training data	ML model	R ²	RMSE	SSE	MAE
180 days	GB-90-10	0.96	0.0640	0.0595	0.0520
	GB-80-20	0.96	0.0720	0.0600	0.0560
	GB-70-30	0.94	0.0840	0.0672	0.0650
	GB-60-40	0.95	0.0700	0.0431	0.0500
	NN-90-10	0.66	0.1400	0.3732	0.1100
	NN-80-20	0.81	0.1200	0.1067	0.0710
	NN-70-30	0.87	0.0860	0.0824	0.0660
	NN-60-40	0.89	0.0990	0.1021	0.0800
	MVL-90-10	0.81	0.1000	0.2929	0.0810
	MVL-80-20	0.80	0.1100	0.2645	0.0890
	MVL-70-30	0.78	0.1200	0.2626	0.0870
	MVL-60-40	0.74	0.1300	0.2802	0.0920
	RF-90-10	0.96	0.0280	0.0246	0.0290
	RF-80-20	0.94	0.0690	0.0391	0.0510
	RF-70-30	0.94	0.0670	0.0398	0.0460
	RF-60-40	0.93	0.0850	0.0644	0.0580

3.2.1. PCE prediction

After comparatively evaluating the performance of ML models, this section validates their ability to predict the temporal behavior of the PCE for an OSC device never seen by the models. In other words, a predictive inference of PCE is obtained for data from a particular OSC that has been omitted in the training and validation phases. Firstly, the models are trained and validated without data of *Cell4* (same example used so far), thus the accuracy metrics are presented in Table 10. Standing out above the others are the GB-90-10 and RF-90-10 models. Secondly, the four trained models presented in Table 10, are queried to get predictive inferences up to 180 days for the unseen OSC, i.e. *Cell4*. Table 11 summarizes these accuracy results for each of these inferences. Again, both in Table 10 (training-validation) and in Table 11 (predictive testing) the highlighted error metrics together with the R^2 values higher than 0.90, are indicative of feasibility to achieve our goal. Finally, Figure 8 provides visual detail for the particular results obtained with one of the best models, GB-90-10, to predict PCE over 180 days. Since the figure only shows the behavior of PCE against the time variable, once again, it is worth emphasizing on the potential of these models to encode accurately the multivariate variations of our dataset for an unknown OSC device.

Table 10: Accuracy metrics of the Machine Learning regression models without training nor validation data of the OSC *Cell4*, which is not seen by the models.

ML model	R^2	RMSE	SSE	MAE
GB-90-10	0.88	0.069	0.0906	0.0600
NN-90-10	0.89	0.095	0.3005	0.0740
MVL-90-10	0.80	0.091	0.7528	0.0790
RF-90-10	0.96	0.071	0.1118	0.050

Table 11: Accuracy metrics of the Machine Learning regression models used as predictors of the PCE for the unseen OSC, *Cell4*.

ML model	R^2	RMSE	SSE	MAE
GB-90-10	0.97	0.055	0.0914	0.0370
NN-90-10	0.80	0.1000	0.1975	0.0800
MVL-90-10	0.90	0.1500	0.4010	0.1500
RF-90-10	0.94	0.0610	0.0674	0.0470

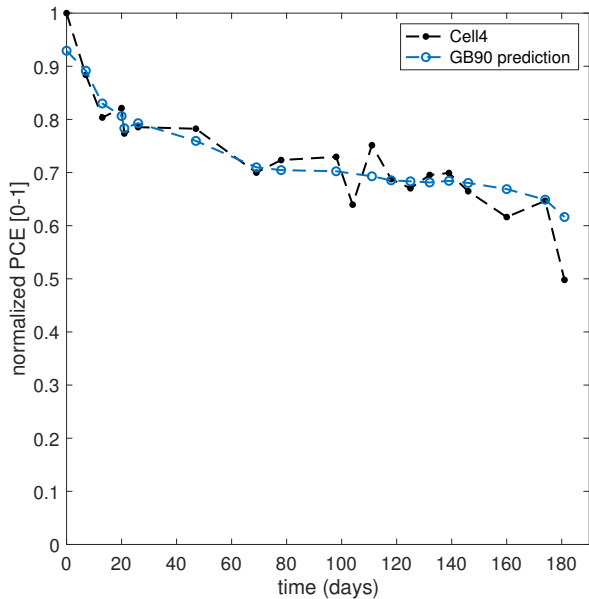


Figure 8: PCE prediction over time with the best Machine Learning regression model (GB-90-10, Table 11) for an OSC not seen during the training neither the validation not the test.

3.2.2. Variable's influence on the PCE

In light of the results obtained in the previous section, it is worthwhile to study some of the top-performing ML models that characterize the behavior of OSCs. In this regard, standardized PFI and SHAP analyses are presented below, by means of Figure 9 and Figure 10, respectively. In this case, the behavior of OSCs is analyzed upon the variables of the dataset, for a temporal scope of up to 30 and 180 days, respectively.

Firstly, Figure 9(a) and Figure 9(b) compare the importance of all the variables without applying PFI filtering, for the best model at 30 and 180 days, in turn. It is confirmed that in initial stages, the effect of time is not clearly relevant on the PCE, compared to the model trained with data of 180 days. The remaining variables have similar implications, being the amount of solvent in the HTL layer, i.e., the amount of PEDOT:PSS, the more significant. Likewise, the P3HT:PCBM ratio also demonstrates certain relevance.

After applying PFI filtering, that is, removing variables with an effect on the R^2 lesser than 4%, it is observed that in models generated with data up to 30 days, in Figure 9(c), the most significant variable is now the P3HT:PCBM ratio, above the amount of solvent in the HTL layer. Meanwhile, in models generated with data up to 180 days, in Figure 9(d), the effect of this quantity is greater. Additionally, dependencies with the value of PCBM are also observed, as it

has more relevance for calculating the P3HT:PCBM ratio, given its non-linear influence since it modulates the value from the denominator.

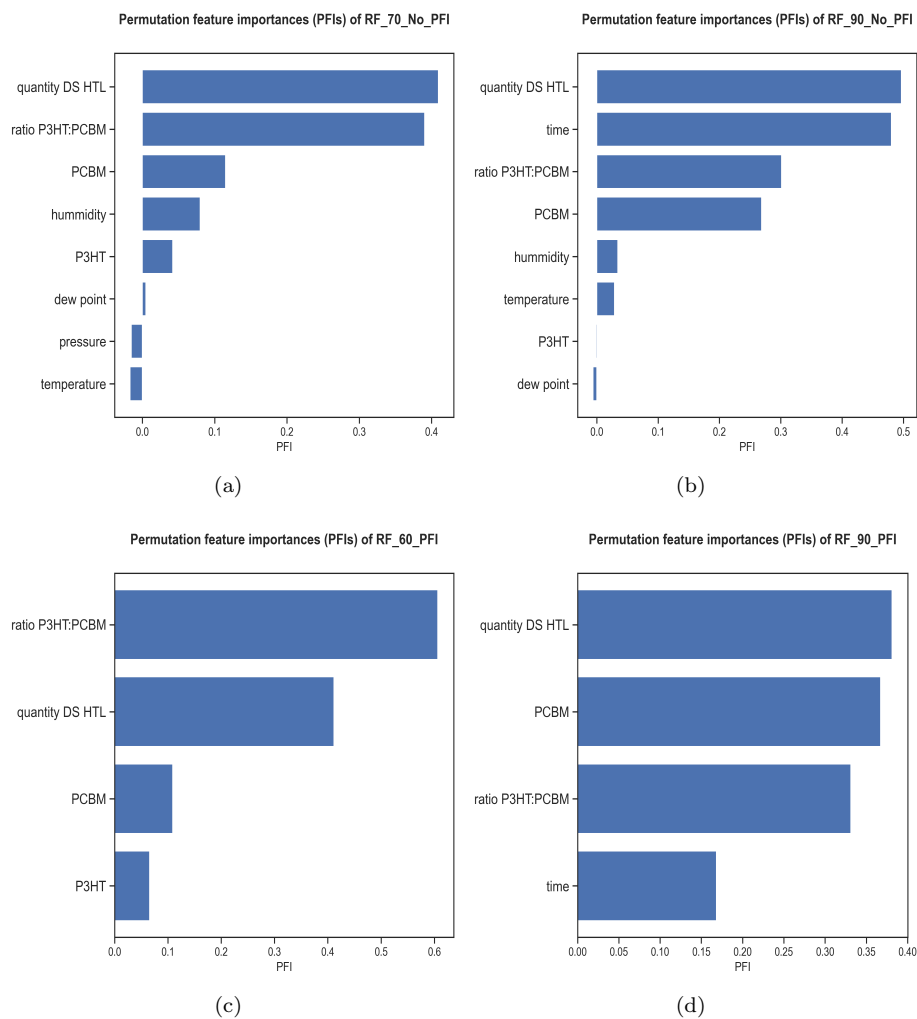


Figure 9: PFI comparison between the best Machine Learning models generated with data up to: 30 days, in (a) and (c); 180 days, in (b) and (d). Variables with less than 4% of contribution to R^2 are filtered out in (c) and (d).

Regarding the SHAP analysis, it proves the extension of the insights previously extracted. When PFI filtering is not applied, Figure 10(a) and Figure 10(b) demonstrate the influence on the model of the amount of solvent PEDOT:PSS in the HTL layer, regardless of whether the model is generated with data up to 30 days or 180 days. However, in the latter case, the P3HT:PCBM ratio also shows greater relevance. As for the environmental conditions (tem-

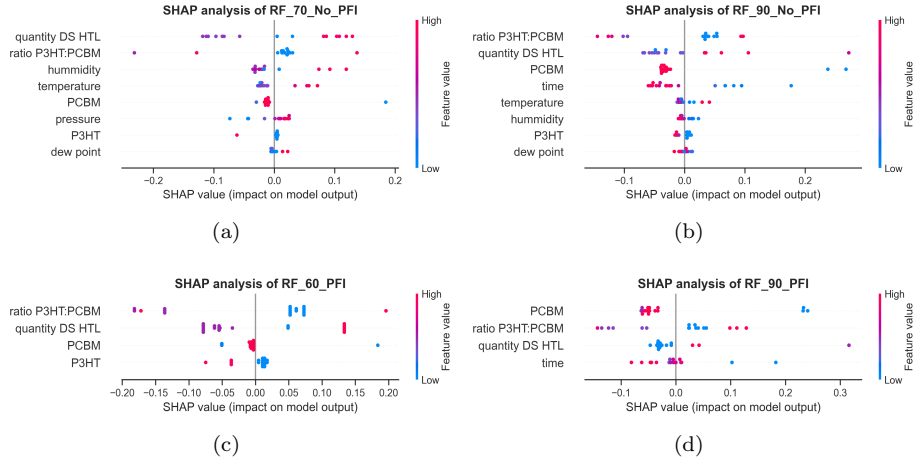


Figure 10: SHAP comparison between the best Machine Learning models generated with data up to: 30 days, in (a) and (c); 180 days, in (b) and (d). Variables with less than 4% of contribution to R^2 are filtered out in (c) and (d).

perature, humidity, dew point, and pressure), it is shown that they do not have wide influence. At initial stages (up to 30 days), there is low variation in these climate conditions, so that further insights should not be trustworthy made. By contrast, when enough time is taken into consideration (up to 180 days), it is confirmed that low humidity proves to be beneficial for these OSCs, which in our geographical location is normally correlated with high temperatures and atmospheric pressures. In a similar manner affects the dew point, which directly correlates with humidity. Nonetheless, the device encapsulation demonstrates that the effect of these variables is minimized, as it will be verified in the PFI analysis.

Finally, after applying PFI filtering, Figure 10(c) and Figure 10(d) highlight the same dependencies, where the effect of the PCBM value on the P3HT:PCBM ratio is again confirmed. As recently mentioned, it is verified that PFI filters out the effect of climate variables during the data acquisition, since it is mitigated by the encapsulation of the devices.

4. Discussion and conclusions

This paper has presented the application of an optimal ML framework to characterize the degradation behavior, in terms of PCE, of OSCs with multi-layer structure ITO/PEDOT:PSS/P3HT:PCBM/Al. A dataset with electrical parameters of these devices has been acquired for more than 180 days, so as to come up with 996 entries, with variability in 7 variables. Through hyper-optimization of a set of well-recognized ML models we have presented an accuracy analysis of different methods, which were fed with OSC data periodized

into sets from 30 to 180 days. The benchmarking has confirmed the validity of models like RF or GB to confer R^2 values over 0.90, reaching in some extents $R^2 \sim 0.96-0.97$. As for the error metrics obtained (RMSE, SSE and MAE), they are trustworthy bounded to $\lesssim 1\%$ of the target value (the PCE) when long term data is used for training. To reinforce the suitability of these ML models, classical LMS regression fitting methods have been presented. They demonstrated inoperability to perform reliably with multivariate models, neither with long-term data, and even less to estimate future values of the target PCE.

By contrast, our ML models offer high feasibility to predict the behavior of unknown OSCs, with accuracy of $R^2=0.97$. Finally, the standardized result report provided by the ML framework, permits obtaining further insights of the dependencies of the variables of the dataset on the degradative behavior the OSCs, as per their importance in the ML models. It has been confirmed the importance of the solvent in the HTL layer, i.e., the amount of PEDOT:PSS. This is explained as the multilayer structure of the OSCs needs a minimum value of PEDOT:PSS to ensure a layer that completely covers the substrate. Moreover, the ratio P3HT:PCBM also exhibits significant importance, being higher values representative of greater impact on the model. It is worth noticing that models with data up to 180 days provide more stable implications in this sense. Finally, it has been validated that variables such as temperature, humidity, dew point and pressure have lesser impact on the models, explained by the encapsulation made to the OSCs during their manufacturing. Overall, this study comes up with robust and reliably ML models that characterize these OSCs in a reproducible, transparent and standardized manner, which are made publicly available.

References

- [1] H. Ritchie, M. Roser, Energy, accessed on 2024-18-03 (2024).
URL <https://ourworldindata.org/energy>
- [2] New Media Consortium, New Media Consortium Horizon Report, accessed on 2024-18-03 (2024).
URL <https://www.nrel.gov/pv/cell-efficiency.html>
- [3] J. H. Seo, H.-D. Um, A. Shukla, I. Hwang, J. Park, Y.-C. Kang, C. S. Kim, M. Song, K. Seo, Low-temperature solution-processed flexible organic solar cells with pfn/agnws cathode, *Nano Energy* 16 (2015) 122–129. doi:10.1016/j.nanoen.2015.06.013.
- [4] N. Yeh, P. Yeh, Organic solar cells: Their developments and potentials, *Renewable and Sustainable Energy Reviews* 21 (2013) 421–431. doi:10.1016/j.rser.2012.12.046.
- [5] A. R. Ayub, W. Akram, M. A. Khan, M. Zeshan, M. Ateeb, U. Yaqoob, M. U. Dad, A. Elmushyakh, A. M. Shawky, J. Iqbal, Designing of asymmetric non-fullerene based acceptor materials by re-modification of spacers with pce for organic solar cell, *Optik* 278 (2023) 170602. doi:10.1016/j.ijleo.2023.170602.

- [6] P. Chiappafreddo, A. Gagliardi, The photovoltaic market facing the challenge of organic solar cells: Economic and technical perspectives, *Transition Studies Review* 17 (2) (2010) 346–355. doi:10.1007/s11300-010-0148-0.
- [7] M. Venkata, A. Agrios, S. Ahmad, *Current and Emerging Technologies and Materials for Solar Power Conversion*, Vol. 1, CRC Press, 2016. doi:10.1201/9781315369853.
- [8] C. J. Brabec, J. A. Hauch, P. Schilinsky, C. Waldauf, Production aspects of organic photovoltaics and their impact on the commercialization of devices, *MRS Bulletin* 30 (1) (2005) 50–52. doi:10.1557/mrs2005.10.
- [9] A. Lusci, G. Pollastri, P. Baldi, Deep architectures and deep learning in chemoinformatics: The prediction of aqueous solubility for drug-like molecules, *Journal of Chemical Information and Modeling* 53 (7) (2013) 1563–1575. doi:10.1021/ci400187y.
- [10] K. Hansen, G. Montavon, F. Biegler, S. Fazli, M. Rupp, M. Scheffler, O. A. von Lilienfeld, A. Tkatchenko, K.-R. Müller, Assessment and validation of machine learning methods for predicting molecular atomization energies, *Journal of Chemical Theory and Computation* 9 (8) (2013) 3404–3419. doi:10.1021/ct400195d.
- [11] M. Rupp, A. Tkatchenko, K.-R. Müller, O. A. von Lilienfeld, Fast and accurate modeling of molecular atomization energies with machine learning, *Phys. Rev. Lett.* 108 (2012) 058301. doi:10.1103/PhysRevLett.108.058301.
- [12] T. Unterthiner, A. Mayr, J. K. Wegner, Deep learning as an opportunity in virtual screening, in: *Deep learning workshop at NIPS*, 2015. URL <https://api.semanticscholar.org/CorpusID:38235267>
- [13] I. Wallach, M. Dzamba, A. Heifets, Atomnet: A deep convolutional neural network for bioactivity prediction in structure-based drug discovery, *ArXiv abs/1510.02855* (2015). doi:10.48550/arXiv.1510.02855.
- [14] J. Hachmann, R. Olivares-Amaya, S. Atahan-Evrenk, C. Amador-Bedolla, R. S. Sánchez-Carrera, A. Gold-Parker, L. Vogt, A. M. Brockway, A. Aspuru-Guzik, The Harvard clean energy project: Large-scale computational screening and design of organic photovoltaics on the world community grid, *The Journal of Physical Chemistry Letters* (17) (2011) 2241–2251. doi:10.1021/jz200866s.
- [15] A. Eibeck, D. Nurkowski, A. Menon, J. Bai, J. Wu, L. Zhou, S. Mosbach, J. Akroyd, M. Kraft, Predicting power conversion efficiency of organic photovoltaics: Models and data analysis, *ACS Omega* 6 (37) (2021) 23764–23775. doi:10.1021/acsomega.1c02156.
- [16] L. Serrano-Lujan, J. M. Cadenas, J. Faxas-Guzman, A. Urbina, Case of study: Photovoltaic faults recognition method based on data mining techniques, *Journal of Renewable and Sustainable Energy* 8 (4) (2016) 043506. doi:10.1063/1.4960410.
- [17] C. Toledo, L. Serrano-Lujan, J. Abad, A. Lampitelli, A. Urbina, Measurement of thermal and electrical parameters in photovoltaic systems for predictive and cross-correlated monitorization, *Energies* 12 (4) (2019). doi:10.3390/en12040668.
- [18] S. A. Lopez, E. O. Pyzer-Knapp, G. N. Simm, T. Lutzow, K. Li, L. R. Seress, J. Hachmann, A. Aspuru-Guzik, The Harvard organic photovoltaic dataset, *Scientific Data* 3 (1) (2016) 160086. doi:10.1038/sdata.2016.86.

- [19] G. J. Moore, O. Bardagot, N. Banerji, Deep transfer learning: A fast and accurate tool to predict the energy levels of donor molecules for organic photovoltaics, *Advanced Theory and Simulations* 5 (5) (2022) 2100511. doi:10.1002/adts.202100511.
- [20] P. Malhotra, S. Biswas, F.-C. Chen, G. D. Sharma, Prediction of non-radiative voltage losses in organic solar cells using machine learning, *Solar Energy* 228 (2021) 175–186. doi:10.1016/j.solener.2021.09.056.
- [21] S. Ryu, Y. Kwon, W. Y. Kim, A Bayesian graph convolutional network for reliable prediction of molecular properties with uncertainty quantification, *Chem. Sci.* 10 (2019) 8438–8446. doi:10.1039/C9SC01992H.
- [22] W. Sun, M. Li, Y. Li, Z. Wu, Y. Sun, S. Lu, Z. Xiao, B. Zhao, K. Sun, The use of deep learning to fast evaluate organic photovoltaic materials, *Advanced Theory and Simulations* 2 (1) (2019) 1800116. doi:10.1002/adts.201800116.
- [23] Y. Miyake, A. Saeki, Machine learning-assisted development of organic solar cell materials: Issues, analyses, and outlooks, *The Journal of Physical Chemistry Letters* 12 (51) (2021) 12391–12401. doi:10.1021/acs.jpcllett.1c03526.
- [24] A. Mahmood, A. Irfan, J.-L. Wang, Machine learning and molecular dynamics simulation-assisted evolutionary design and discovery pipeline to screen efficient small molecule acceptors for PTB7-Th-based organic solar cells with over 15% efficiency, *J. Mater. Chem. A* 10 (2022) 4170–4180. doi:10.1039/D1TA09762H.
- [25] A. Mahmood, J.-L. Wang, Machine learning for high performance organic solar cells: current scenario and future prospects, *Energy Environ. Sci.* 14 (2021) 90–105. doi:10.1039/D0EE02838J.
- [26] J. D. Velasquez, L. Cadavid, C. J. Franco, Intelligence techniques in sustainable energy: Analysis of a decade of advances, *Energies* 16 (19) (2023). doi:10.3390/en16196974.
- [27] M.-G. Ju, M. Chen, Y. Zhou, J. Dai, L. Ma, N. P. Padture, X. C. Zeng, Toward eco-friendly and stable perovskite materials for photovoltaics, *Joule* 2 (7) (2018) 1231–1241. doi:10.1016/j.joule.2018.04.026.
- [28] A. Mahmood, Y. Sandali, J.-L. Wang, Easy and fast prediction of green solvents for small molecule donor-based organic solar cells through machine learning, *Phys. Chem. Chem. Phys.* 25 (2023) 10417–10426. doi:10.1039/D3CP00177F.
- [29] M. Jobayer, M. A. H. Shaikat, M. Naimur Rashid, M. R. Hasan, A systematic review on predicting pv system parameters using machine learning, *Heliyon* 9 (2023). doi:10.1016/j.heliyon.2023.e16815.
- [30] Y. Tang, K. Yang, S. Zhang, Z. Zhang, Photovoltaic power forecasting: A dual-attention gated recurrent unit framework incorporating weather clustering and transfer learning strategy, *Engineering Applications of Artificial Intelligence* 130 (2024) 107691. doi:10.1016/j.engappai.2023.107691.
- [31] A. E. Gürel, Ü. Ağbulut, H. Bakir, A. Ergün, G. Yildiz, A state of art review on estimation of solar radiation with various models, *Heliyon* 9 (2) (2023). doi:10.1016/j.heliyon.2023.e13167.
- [32] D. C. Nguyen, Y. Ishikawa, On predicting annual output energy of 4-terminal perovskite/silicon tandem pv cells for building integrated photovoltaic application using machine learning, *Heliyon* 9 (7) (2023). doi:10.1016/j.heliyon.2023.e18097.

- [33] J. Yu, Z. Wang, A. Majumdar, R. Rajagopal, Deepsolar: A machine learning framework to efficiently construct a solar deployment database in the united states, *Joule* 2 (12) (2018) 2605–2617. doi:10.1016/j.joule.2018.11.021.
- [34] H. Uzen, M. Turkoglu, M. Aslan, D. Hanbay, Depth-wise squeeze and excitation block-based efficient-unet model for surface defect detection, *The Visual Computer* (2022) 1745–1764doi:10.1007/s00371-022-02442-0.
- [35] D. Dwivedi, K. V. S. M. Babu, P. K. Yemula, P. Chakraborty, M. Pal, Identification of surface defects on solar pv panels and wind turbine blades using attention based deep learning model, *Engineering Applications of Artificial Intelligence* 131 (2024) 107836. doi:10.1016/j.engappai.2023.107836.
- [36] M. O. Yildirim, E. C. Gok Yildirim, E. Eren, P. Huang, M. P. U. Haris, S. Kazim, J. Vanschoren, A. Uygun Oksuz, S. Ahmad, Automated machine learning approach in material discovery of hole selective layers for perovskite solar cells, *Energy Technology* 11 (1) (2023) 2200980. doi:10.1002/ente.202200980.
- [37] M. K. Park, J. M. Lee, W. H. Kang, J. M. Choi, K. H. Lee, Predictive model for PV power generation using RNN (LSTM), *Journal of Mechanical Science and Technology* 35 (2) (2021) 795–803. doi:10.1007/s12206-021-0140-0.
- [38] M. Mammeri, L. Dehimi, H. Bencherif, M. Amami, S. Ezzine, R. Pandey, M. K. Hossain, Targeting high performance of perovskite solar cells by combining electronic, manufacturing and environmental features in machine learning techniques, *Heliyon* 9 (11) (2023). doi:10.1016/j.heliyon.2023.e21498.
- [39] M.-H. Lee, Interpretable machine learning model for the highly accurate prediction of efficiency of ternary organic solar cells based on nonfullerene acceptor using effective molecular descriptors, *Solar RRL* 7 (14) (2023) 2300307. doi:10.1002/solr.202300307.
- [40] Z. Zhang, H. Wang, T. J. Jacobsson, J. Luo, Big data driven perovskite solar cell stability analysis, *Nature Communications* 13 (1) (2022) 7639. doi:10.1038/s41467-022-35400-4.
- [41] Y. Zhang, H. Yi, A. Iraqi, J. Kingsley, A. Buckley, T. Wang, D. G. Lidzey, Comparative indoor and outdoor stability measurements of polymer based solar cells, *Scientific Reports* 7 (1) (2017) 1305.
- [42] I. Borazan, A study about lifetime of photovoltaic fibers, *Solar Energy Materials and Solar Cells* 192 (2019) 52–56. doi:10.1016/j.solmat.2018.12.003.
- [43] B. N. N. Alsulami, T. W. David, A. Essien, S. Kazim, S. Ahmad, T. J. Jacobsson, A. Feeney, J. Kettle, Application of large datasets to assess trends in the stability of perovskite photovoltaics through machine learning, *J. Mater. Chem. A* 12 (2024) 3122–3132. doi:10.1039/D3TA05966A.
- [44] S. Jaman, M. B. Asfia, M. Abdur Rashid, Band gap engineering and enhanced optoelectronic performance by varying dopant concentration in RbSr_{1-x}Sn_xCl₃: Ab-initio, *Physica B: Condensed Matter* 678 (2024) 415779. doi:10.1016/j.physb.2024.415779.
- [45] A. R. Tetreault, I. Lopez-Carreón, M. Riahinezhad, E. Esmizadeh, P. Collins, K. A. Zarasvand, N. Vivekanandan, A. Mandlik, M. Fernandes, K. Golovin, T. P. Bender, Assessing individual material degradation toward organic solar cells using accelerated nanolayer lifetime protocols: Implications for solar cell longevity, *ACS Applied Nano Materials* 7 (4) (2024) 4182–4198. doi:10.1021/acsnm.3c05732.

- [46] I. C. Ghosekar, G. C. Patil, Performance analysis and thermal reliability study of multilayer organic solar cells, *IEEE Transactions on Device and Materials Reliability* 19 (3) (2019) 572–580. doi:10.1109/TDMR.2019.2933312.
- [47] B. P. Kore, M. Jamshidi, J. M. Gardner, The impact of moisture on the stability and degradation of perovskites in solar cells, *Material Advances* (2024). doi:10.1039/D3MA00828B.
- [48] A. R. J. Dalmau D, ROBERT: Bridging the gap between machine learning and chemistry., *ChemRxiv*. (2023). doi:10.26434/chemrxiv-2023-k994h.
- [49] M. Bozorg, A. Bracale, P. Caramia, G. Carpinelli, M. Carpita, P. De Falco, Bayesian bootstrap quantile regression for probabilistic photovoltaic power forecasting, *Protection and Control of Modern Power Systems* 5 (1) (2020) 21. doi:10.1186/s41601-020-00167-7.
- [50] T. O. Owolabi, K. O. Akande, S. O. Olatunji, N. Aldhafferi, A. Alqahtani, Modeling energy band gap of doped TiO₂ semiconductor using homogeneously hybridized support vector regression with gravitational search algorithm hyperparameter optimization, *AIP Advances* 7 (11) (2017) 115225. doi:10.1063/1.5009693.
- [51] P. Wolf, V. Benda, Identification of pv solar cells and modules parameters by combining statistical and analytical methods, *Solar Energy* 93 (2013) 151–157. doi:10.1016/j.solener.2013.03.018.
- [52] P. Holland, R. E. Welsch, Robust regression using iteratively reweighted least-squares, *Communications in Statistics-theory and Methods* 6 (1977) 813–827. URL <https://api.semanticscholar.org/CorpusID:122208291>
- [53] F. Pedregosa, G. Varoquaux, A. Gramfort, V. Michel, B. Thirion, O. Grisel, M. Blondel, P. Prettenhofer, R. Weiss, V. Dubourg, J. Vanderplas, A. Passos, D. Cournapeau, M. Brucher, M. Perrot, Édouard Duchesnay, Scikit-learn: Machine learning in python, *Journal of Machine Learning Research* 12 (85) (2011) 2825–2830. URL <http://jmlr.org/papers/v12/pedregosa11a.html>